PHILOSOPHICAL TRANSACTIONS A

rsta.royalsocietypublishing.org

Research

Cite this article: Shur VYa, Akhmatkhanov AR. 2018 Domain shape instabilities and dendrite domain growth in uniaxial ferroelectrics. *Phil. Trans. R. Soc. A* **376**: 20170204.
http://dx.doi.org/10.1098/rsta.2017.0204

Accepted: 25 August 2017

One contribution of 16 to a theme issue 'From atomistic interfaces to dendritic patterns'.

Subject Areas:
nanotechnology

Keywords:
ferroelectrics, ferroelectric domain structure, domain kinetics, lithium niobate, lithium tantalate

Author for correspondence:
Vladimir Ya. Shur
e-mail: Vladimir.Shur@urfu.ru

THE ROYAL SOCIETY PUBLISHING

Domain shape instabilities and dendrite domain growth in uniaxial ferroelectrics

Vladimir Ya. Shur and Andrey R. Akhmatkhanov

Ferroelectric Lab, School of Natural Sciences and Mathematics, Ural Federal University, 51 Lenin Avenue, Ekaterinburg 620000, Russia

VYaS, 0000-0002-6970-7798

The effects of domain wall shape instabilities and the formation of nanodomains in front of moving walls obtained in various uniaxial ferroelectrics are discussed. Special attention is paid to the formation of self-assembled nanoscale and dendrite domain structures under highly non-equilibrium switching conditions. All obtained results are considered in the framework of the unified kinetic approach to domain structure evolution based on the analogy with first-order phase transformation.

This article is part of the theme issue 'From atomistic interfaces to dendritic patterns'.

1. Introduction

(a) Domain shapes in ferroelectrics

Recent research into ferroelectric domain structure evolution at the nanoscale revealed a self-assembled domain growth, domain shape instabilities and formation of self-similar dendrite domain patterns. It should be noted that the domain patterns obtained demonstrated a complicated shape with pronounced scaling invariance, and therefore possess fractal geometry [1]. Thus, the domain structure of uniaxial ferroelectrics can be considered as the model for investigation of dendrite growth.

The kinetic approach to domain structure evolution in ferroelectrics, based on the analogy with first-order phase transition, allows the experimentally realized formation of various metastable domain structures to be explained with energy essentially exceeding that of the equilibrium [2–4]. Compensation of the depolarization field by fast external and slow bulk screening processes permits stabilization of almost any domain pattern. Moreover, it has been shown that

screening retardation drastically changes the evolution of the domain structure [3–5]. Realization of the highly non-equilibrium switching conditions characterized by ineffective bulk screening leads to self-assembled formation and evolution of nanodomain structures of complicated shapes [3,6–9].

We have studied domain structure evolution by joint application of optical microscopy, confocal Raman microscopy (CRM), scanning electron microscopy (SEM) and piezoresponse force microscopy (PFM) for domain visualization. We chose high-quality uniaxial ferroelectric crystals—lithium niobate $LiNbO_3$ (LN) and lithium tantalate $LiTaO_3$ (LT)—as the model materials. The main ideas of the kinetic approach to domain structure evolution are described briefly. The crucial role of the residual depolarization field in the formation of self-assembled micro- and nanodomain structures is demonstrated. The effects of domain wall shape instabilities and the formation of nanodomains in front of moving walls are discussed. Special attention is paid to several scenarios of formation of self-assembled nanoscale dendrite domain structures under highly non-equilibrium switching conditions. All obtained results are considered in the framework of the described kinetic approach.

(b) Domain structure evolution during polarization reversal

Evolution of the domain structure during polarization reversal is governed by nucleation processes of different dimensionalities. The nuclei represent the smallest domains with orientation of the spontaneous polarization determined by the direction of the applied electric field. The appearance of new domains is due to three-dimensional (3D) nucleation. The domain wall motion is the result of two-dimensional (2D) nucleation, leading to the generation of the elementary steps (pair of kinks) at the wall, and one-dimensional (1D) nucleation, leading to kink motion along the wall. The probabilities of all nucleation processes are governed by the local value of the projection of the electric field on the crystal polar axis averaged over the nuclei volume [4,5].

In situ domain visualization allowed us to separate the five main stages of structure evolution during polarization reversal from the single-domain state: (i) nucleation of new domains, (ii) forward domain growth, (iii) sideways domain growth, (iv) domain coalescence, and (v) spontaneous backswitching (figure 1) [5].

'Nucleation of new domains' is the most difficult to study experimentally as it requires visualization of the isolated nanodomains. It is still under discussion whether the initial domain state is a single domain or contains the residual nanodomains [3,4]. In the latter case, the appearance of new domains represents a transformation of the invisible nanoscale domains into visible ones as a result of domain growth. The new needle-like domains appeared usually at the polar surface (figure 1*a*). The domains with the same initial orientation as the spontaneous polarization exist after termination of the switching pulse due to incomplete domain merging and spontaneous backswitching [6,10].

'Forward domain growth' represents a relatively fast expansion of the needle-like domains that appeared in the polar direction as a result of the rapid motion of the domain tip through the sample (figure 1*b*). Direct observation of this stage is still poorly explored as it encounters experimental difficulties due to the requirement for domain visualization in the bulk with high spatial resolution [11–13]. Forward growth is considered as step generation at the surface, and kink motion as step generation in the polar direction [2,3].

The 'sideways domain growth' stage is the best studied experimentally by *in situ* methods. The domain growth is achieved through domain wall motion in the direction transversal to the polar one (figure 1*c*). The shape of the isolated domains depends crucially on the switching conditions [4,10,14–17].

'Coalescence of the residual domains' (merging) (figure 1*d*) is characterized by deceleration of the approaching domain walls, which is caused by electrostatic interaction resulting usually in the formation of the residual nanodomain arrays and net structures [18].

'Spontaneous backswitching' (flip-back) after electric field switch-off represents partial restoration of the initial domain state by backward wall motion and appearance of the domains

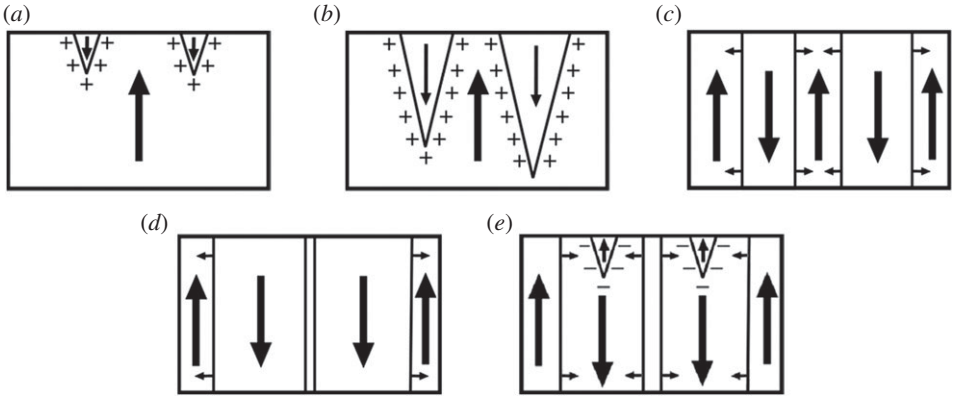

Figure 1. The main stages of domain structure evolution during polarization reversal from the single-domain state [5]. (*a*) Nucleation of new domains, (*b*) forward domain growth, (*c*) sideways domain growth, (*d*) domain coalescence and (*e*) spontaneous backswitching.

with the same initial direction as the spontaneous polarization (figure 1*e*). Backswitching is induced by the residual depolarization field, which is abnormally high and allows the highly non-equilibrium switching condition to be realized, leading to the formation of concentric domain structures for local switching [19] and self-assembled dendrite nanodomain structures for switching by uniform fields [3,6,8,10].

2. General consideration: kinetic approach

All the stages of the domain structure evolution during polarization reversal can be considered within the frame of the unified approach as a manifestation of the various nucleation processes similar to the first-order phase transformations, such as crystal growth [20,21]. It was noted by Cahn that the mechanism of crystal growth could be applied while considering 'not only surfaces between a solid and a fluid, but also interfaces in a crystalline medium when the same lattice extends to the both phases as in … ferroelectric domain walls' [22]. Within this approach, the neighbouring domains are similar to the volumes of different phases divided by interfaces (domain walls).

Domain structure evolution has to be considered as a result of thermally activated generation of 1D, 2D and 3D nuclei (1D-, 2D- and 3D-nucleation) with preferred orientation of the spontaneous polarization (figure 1*a*). It was demonstrated that such a kinetic approach is fruitful in the explanation of the complicated domain shapes [3–5].

Wall motion is achieved through 1D- and 2D-nucleation. The elementary one-unit-cell steps (kink pairs) are generated at the domain wall by 2D-nucleation. The subsequent kink motion along the wall is the result of 1D-nucleation. The nucleation probability determining the switching rate is governed by the local value of the electric field averaged over the nucleus size ('local field', E_{loc}) [1]. In a ferroelectric capacitor, E_{loc} contains four components: (i) the external field (E_{ex}) applied by the electrodes, (ii) the depolarization field (E_{dep}) produced by the bound charges and that is dependent on the domain shape and size, (iii) the external screening field (E_{exscr}) originating from the charge redistribution at the electrodes, and (iv) the bulk screening field (E_{bscr}) governed by bulk screening processes,

$$E_{\mathrm{loc}}(r,t) = E_{\mathrm{ex}}(r) + E_{\mathrm{dep}}(r,t) + E_{\mathrm{exscr}}(r,t) + E_{\mathrm{bscr}}(r,t). \tag{2.1}$$

The screening processes are crucial for the formation and stabilization of the domain patterns. The thermodynamic approach considers the formation of the equilibrium domain structures with the minimal value of the sum of depolarization energy and the energy of the domain walls [20,23,24]. However, screening diminishes the depolarization energy and leads to the

formation of the metastable domain patterns with energy considerably exceeding that of the equilibrium ones [3–5]. The lifetime of the metastable domain structures can be long. One of the consequences of the screening effect is related to the formation of the charged domain walls with extremely high additional input of the depolarization energy caused by the bound charges [25,26].

3. Screening ineffectiveness

Depolarization field screening is crucial for the stabilization of the reversed domain state. The screening processes demonstrate a wide range of characteristic times. It is necessary to distinguish the external and bulk screening mechanisms. Fast external screening, achieved through charge redistribution at the electrodes, possesses characteristic times ranging from nanoseconds to microseconds. However, this fast screening cannot compensate E_{dep} completely due to the existence of the intrinsic or artificial dielectric surface layer in any ferroelectric capacitor [2,4,27,28]. Therefore, a bulk residual depolarization field E_{rd} remains. Its value is by several orders of magnitude less than E_{dep}, but it is close to the experimentally observed threshold fields E_{th}. Incomplete screening during switching leads to deceleration of the domain wall motion. Retardation of the bulk screening changes the domain structure evolution.

The following three groups of bulk screening mechanisms can be considered: (i) redistribution of the bulk charges [2,27], (ii) reorientation of the defect dipoles [29], and (iii) injection of the carriers from the electrode through the dielectric gap [30]. All the bulk screening mechanisms are comparatively slow with characteristic times ranging from milliseconds to days and months. Retardation of the bulk screening leads to the realization of the non-equilibrium switching conditions.

The ratio between the switching rate $(1/t_s)$ and the bulk screening rate $(1/\tau_{scr})$, which is called the screening ineffectiveness $R = \tau_{scr}/t_s$, can be used for quantitative characterization of the screening efficiency [3,4]. Three ranges of screening ineffectiveness can be distinguished: (i) $R \ll 1$ for 'complete screening', (ii) $R \sim 1$ for 'incomplete screening', and (iii) $R \gg 1$ for 'ineffective screening'. For incomplete screening, suppression of the step generation at the wall leads to deceleration of the wall motion and to the appearance of the domain shape instabilities, such as the finger-type structure (fingering) [3,4]. Ineffective screening leads to the termination of the classical wall motion by step generation and kink motion and to abnormal domain kinetics (discrete switching), leading to the formation of self-organized dendrite nanodomain structures [3,5].

We will consider the formation of dendrite domain structures caused by ineffective screening obtained by (i) the creation of the artificial surface dielectric gap by deposition of the dielectric or by proton exchange (PE) and (ii) spontaneous backswitching.

4. Studied materials

We have studied the domain shape instabilities and dendrite growth in LN and LT single crystals, which are the model materials.

LN and LT in the ferroelectric phase belong to the rhombohedral (trigonal) space group R3c with C_{3v} symmetry. Both crystals are uniaxial ferroelectrics possessing a domain structure with 180° walls only. The optical contrast caused by the residual electric field in the vicinity of the domain walls allows the *in situ* optical visualization of the domain structure evolution to be realized.

Congruent, stoichiometric and MgO-doped representatives of the LN and LT family with essentially different parameters have been investigated. For congruent LN (CLN) and LT (CLT), the threshold fields reach 210 kV cm^{-1} at room temperature (RT) [31]. The stoichiometric LN (SLN) and LT (SLT) possess essentially lower threshold fields and substantially different domain kinetics [32,33]. Practical reasons stimulated our study of domain evolution in MgO-doped LN and LT crystals (MgO : LN and MgO : LT).

Switching experiments have been carried out in single-domain wafers cut perpendicular to the polar axis with thickness ranging from 0.2 to 2 mm and an average roughness of polar surfaces of about 1 nm. Electrodes of liquid electrolyte (water solution of LiCl) and evaporated films of Cr or ITO were used for field applications.

5. Methods of domain visualization

A number of different methods have been widely used for visualization of the static domain patterns in ferroelectrics [34,35]. We shall discuss briefly the most important methods applied in the reviewed experiments: optical microscopy, CRM, SEM and PFM. Unique information about the micro- and nanodomain structures can be extracted due to the synergetic effect of the joint application of these methods. The visualization methods can be divided into two groups: (i) after revealing the domain pattern by selective chemical etching and (ii) without any surface treatment. It is clear that any treatment is undesirable as it can change the domain pattern [36].

Selective chemical etching is the universal technique used in ferroelectrics for revealing the surface domain pattern. The inherent significant difference in the etching rate for neighbouring domains leads to the formation of the surface relief with steps at the domain walls. Visualization of the revealed domain pattern can be performed by optical microscopy and SEM. The surface relief can be measured by the contact mode of atomic force microscopy (AFM) with high spatial resolution [34,35,37,38].

The linear electro-optic effect allows the domains and/or domain walls to be visualized without etching. In uniaxial crystals, the field applied along the polar axis induces a difference in the refractive indices of neighbouring domains, which allows the domains with neutral and charged walls to be visualized using polarized and phase contrast modes. The optical microscopy methods allow *in situ* visualization of the domain structure evolution with high temporal resolution limited by the frequency of the video camera. The diffraction-limited spatial resolution of optical microscopy is about 400 nm.

PFM is applied for domain visualization at the surface with nanoscale resolution by local application of the AC electric field using a conductive tip. The local values of the amplitude and phase of the piezoelectric response are recorded during scanning. The spatial distribution of the phase signal allows the domain contrast to be obtained, whereas the amplitude allows the domain walls to be visualized. PFM spatial resolution ranges typically from 10 to 30 nm [37–44].

CRM enables visualization of the ferroelectric domain in the bulk by recording the Raman spectra collected subsequently from tiny spots of the sample during scanning [45–49]. The change of the phonon modes in the vicinity of the domain walls leads to local variation in position and/or intensity of certain Raman lines [47,49–52]. For domain wall visualization, the spatial dependence of the chosen spectral parameter obtained during 2D scanning is converted into 2D digital arrays and represented in pseudo-colour images [53]. CRM allows the domains in the bulk to be visualized with a spatial resolution below the diffraction limit (250–300 nm) [45,48].

6. Domain wall motion

The shape and orientation of the moving domain wall depend strongly on the position of the nucleation sites. The nucleation process (step generation) can be stochastic or determined.

Stochastic nucleation with random positions of the nucleation sites is the classical approach to the problem of wall motion [21,54], assuming that in the homogeneous field the step generation along the wall is equiprobable. In this case, the rounded shape of the isolated domains does not follow crystal symmetry, and the wall deceleration by local pinning centres is ineffective [54]. However, in some ferroelectrics under usual switching conditions, the isolated polygon domains appeared with walls oriented along definite crystallographic directions. The walls of the hexagonal domains in LN are strictly oriented along three Y directions. Such behaviour is due to the prevalence of the 'determined nucleation'-step generation at the polygon vertices only and kink motion in the proper crystallographic directions [3–5]. This effect, which is

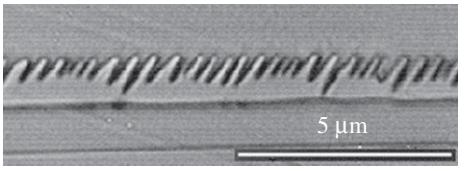

Figure 2. Instability of the domain wall shape showing formation of sub-micrometre fingers. CLN with an artificial dielectric layer. Optical microscopy, with a domain structure revealed by etching. (Reprinted with permission from Shur [3]. Copyright © 2005, Wiley-VCH Verlag GmbH & Co. KGaA.)

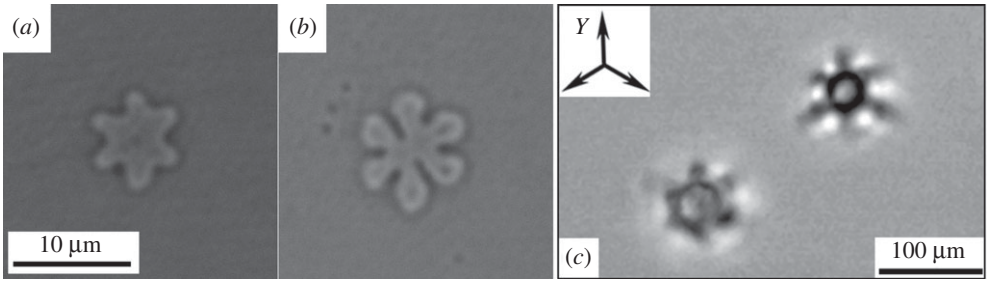

Figure 3. Domain shape instability (*a*,*b*) in SLT and (*c*) in CLN with a PE layer. $E = 22.0$ kV mm^{-1}. Optical microscopy, transmitted light, phase contrast. ((*a*,*b*) Reprinted from Shur *et al.* [55] under CC Attribution 3.0 license.)

caused by screening retardation, leads to the formation of field singularities at the vertices and to a local increase in the step generation probability.

When the classical step-by-step wall motion is completely suppressed due to the ineffective screening of the depolarization field, the alternative mechanism of ongoing switching caused by fluctuations of the planar wall shape can be realized. This mechanism leads to a loss of the domain wall shape stability and to the formation of the self-assembled domain structure with sub-micrometre fingers (figure 2) [3].

The fluctuation of the domain wall shape leading to the formation of a ledge at the domain wall (so-called finger) is oriented along the proper crystallographic direction. The correlated nucleation effect stimulates the generation of neighbouring fingers, leading to the self-organized formation of the quasi-regular finger structure (figure 2).

Domain shape instability during isolated domain growth was revealed in SLT crystals [55]. The process started from the growth of a hexagon. The formation of six bumps at the domain vertices was obtained for domain diameters above 3–5 µm (figure 3*a*). The formed bumps grew in the *Y* directions without merging (figure 3*b*).

The formation of fingers at the vertices was investigated *in situ* by optical microscopy in CLN with a non-polar PE layer (figure 3*c*). It was shown that the polarization reversal process at low field ($E = 21.0$ kV mm^{-1}) started with the appearance and growth of the isolated hexagonal domains, similar to conventional switching. The intensive nucleation at the hexagon vertices at higher field ($E = 22.0$ kV mm^{-1}) led to the lack of domain shape stability for domain sizes above 20 µm and to the formation of domain fingers at all six vertices (figure 3*c*) [56].

7. Self-assembled nanoscale domain structures

(a) Correlated nucleation

Formation of the self-assembled domain structures is caused by correlated nucleation [2,18,56–58]. The origin of the effect is the appearance of the local field maximum in front of the moving domain wall because of ineffective screening in the ferroelectric capacitor with a surface dielectric

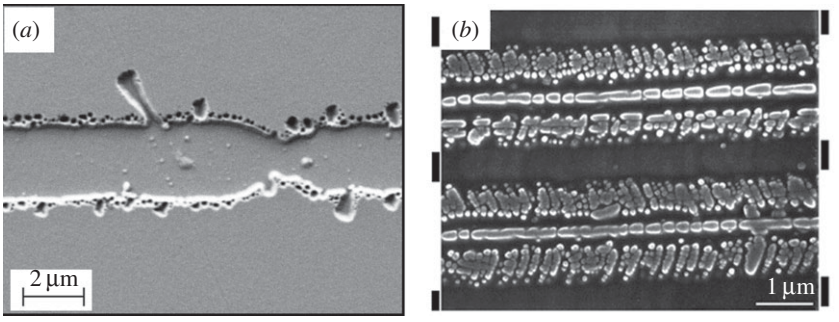

Figure 4. (*a*) The array of needle-like domains formed along the domain wall. CLN after pulse laser heating. (*b*) Nanodomain arrays in periodically poled CLN oriented along the *Y*+ directions. *Z*+ view. SEM images of domain patterns revealed by etching. ((*b*) Reprinted with permission from Shur *et al.* [6]. Copyright © 2000, AIP Publishing LLC.)

gap [2,57,58]. It was shown by computer simulation that the local electrical field maximum is situated near the surface at a distance from the wall that is nearly equal to the thickness of the above dielectric gap L [3,4]. The field singularity changes the domain evolution scenario. It was mentioned above that the trail of the residual field terminates the wall motion by step generation. On the other hand, the field singularity leads to the appearance of isolated nanodomains in front of the moving wall. The nanodomains cannot spread out due to the effect of the residual depolarization field. The decrease of the electric field in the vicinity of the isolated domain initiates domain formation at a given distance from each other. Thus, the quasi-regular array of needle-like micro- or nanodomains aligns along the wall (figure 4*a*).

It has been shown by simulation that the new field maximum appears at almost the same distance from the first domain array, thus initiating the formation of the second one. This reproducible process leads to fast self-maintained enlarging of the quasi-regular domain structure. It has been shown experimentally that the self-assembled structures can cover areas of millimetres squared. The correlated nucleation effect increases for ineffective screening. The period of the quasi-regular structures can be adjusted by changing the artificial dielectric gap thickness.

(b) Nanodomain arrays

Correlated nucleation plays the most important role during backswitching in LN after abrupt external field switch-off. This effect can be attributed to the very high value of spontaneous polarization in LN, leading to the extremely high value of the bulk screening field. After external field switch-off, the local field changes sign, leading to spontaneous backswitching [6,10].

It has been shown experimentally that backward wall motion is achieved through enlarging the self-assembled nanodomain structures (figure 4*b*). For the first time, the formation of nanodomain arrays has been revealed during backswitch poling in CLN in the vicinity of the stripe electrodes under the artificial dielectric layer [3,6,10]. The arrays that are produced are oriented along the *Y*- and *X*-crystallographic directions and consist of 30–100-nm-diameter needle-like domains with charged domain walls (figure 4*b*).

The dense self-assembled structure of the nanodomain rays was observed in CLN with a polar surface modified by PE (figure 5) [19,56]. The structure appeared between approaching walls of two large hexagonal domains. Analysis of the set of CRM domain images obtained at different depths revealed the main stages of structure formation. At the beginning, oriented growth along the *Y* direction of the nanodomain chains connecting the approaching domains prevailed (figure 5*a*). Furthermore, arrays of the first generation merged into domain rays (trunks). Finally, branching (growth of the short domain arrays) started from the primary trunks (figure 5*b*). Branching with subsequent merging resulted in the formation of a very dense pattern of nanodomain rays close to the modified surface (figure 5*c*).

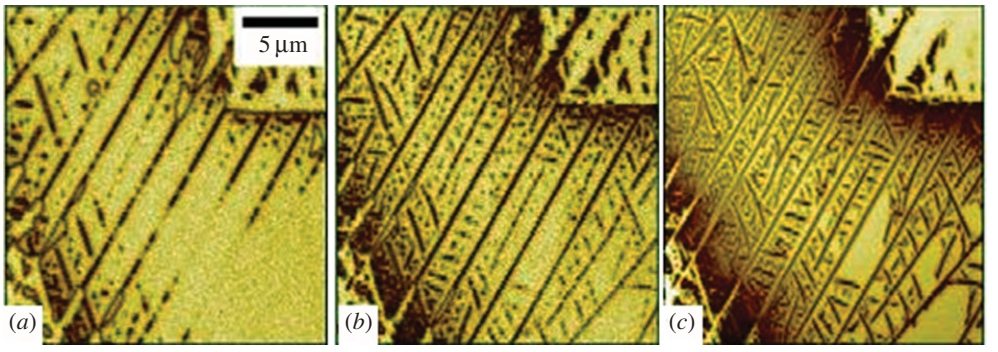

Figure 5. Self-assembled nanodomain rays in CLN with a surface layer modified by PE. CRM images at different depths obtained from a modified surface: (*a*) 67.9 µm, (*b*) 22.6 µm and (*c*) at the surface. (Online version in colour.)

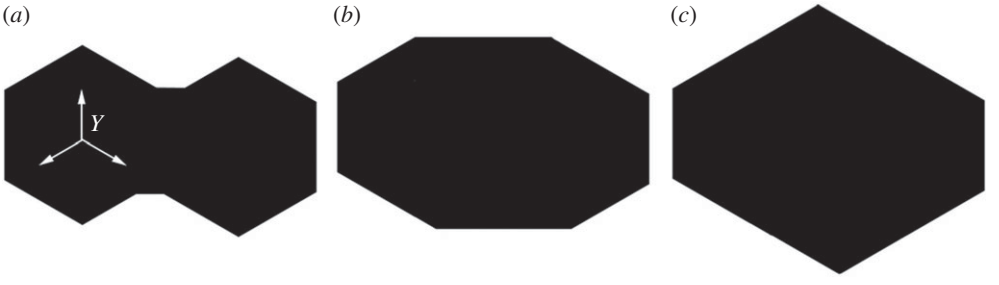

Figure 6. (*a–c*) Scheme of the domain shape stability effect. The main stages of the domain shape recovering after merging. (Reprinted with permission from Shur *et al.* [59]. Copyright © 2013, AIP Publishing LLC.)

8. Shape of the isolated domains

The hexagonal shape of the isolated domains in LN and SLT crystals for switching with effective screening is very stable [59]. It recovers in a short time after domain merging (figure 6). Three stages of shape evolution can be distinguished. First, a polygon with two concave angles, 10 *Y* walls and two *X* walls ($10Y + 2X$), appeared just after merging (figure 6*a*). Second, fast overgrowing of the concave angles leads to a polygon domain shape with convex angles only ($6Y + 2X$) (figure 6*b*). Finally, the hexagonal domain shape ($6Y$) recovers (figure 6*c*). Such a recovering process leads to domain shape stability [59]. Eventually, the hexagonal domain shape with *Y*-oriented walls prevails in LN even at the stage of domain merging. The obtained overgrowing of the concave angles occurs due to essentially faster motion of the *X* walls when compared with the *Y* ones for the determined nucleation mechanism [5].

The domain shape evolution after merging changes drastically for stochastic nucleation, which can be realized for switching at temperatures above 230°C. The continuation of the independent domain growth after merging leads to the formation of the complicated domain shapes with concave angles (figure 7). In such cases, the 'branched growth' of the chains of isolated nanodomains after they merge leads to the formation of dendrite structures [60].

9. Dendrite domain structures

The formation of the complex self-organized domain structures with a dendrite-like shape was observed during switching with ineffective screening. The obtained process was governed by anisotropy of the nucleation and kink motion along the wall caused by anisotropy of

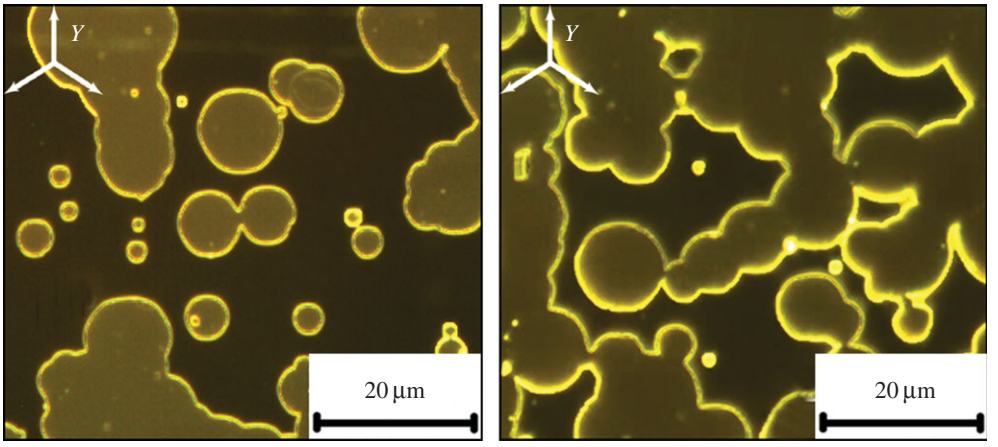

Figure 7. Optical domain images in LT revealed by selective chemical etching after partial polarization reversal at an elevated temperature, $T = 250^{\circ}$C. (Reprinted with permission from Shur *et al.* [60]. Copyright © 2012, AIP Publishing LLC.) (Online version in colour.)

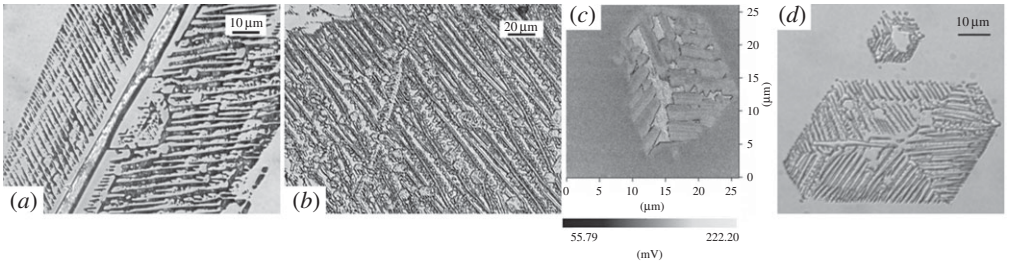

Figure 8. Dendrite domain structures formed as a result of backswitching (*a,b,d*) in MgO : LN with an artificial dielectric layer. Optical observation of the domains revealed by etching (*c*) in CLN (AFM image). (Reprinted with permission from Shur [3]. Copyright © 2005, Wiley-VCH Verlag GmbH & Co. KGaA.)

depolarization field screening by the predominately anisotropic jump-like conductivity [61]. Several mechanisms of dendrite domain growth were revealed: (i) fingering representing the loss of wall shape stability similar to viscous fingers [1], (ii) branching by the formation of new arrays starting from the initial one, and (iii) formation of the residual domain structures during spontaneous backswitching.

The non-equilibrium switching conditions are easily achieved during spontaneous backswitching after abrupt switch-off of the external electric field. In this case, screening retardation leads to the formation of a strong switching field produced by an uncompensated depolarization field. The fast backward motion of the wall as a whole terminates after a small backward shift under the action of the residual depolarization field that appears [3,4]. It was shown in MgO : LN that the backswitched poling by fast switch-off of the uniform electric field produced by continuous electrodes created the quasi-regular domain structures consisting of the stripe-like domains (figure 8). This structure demonstrated three alternative orientations of the stripes along the *Y* directions realized in its different regions (figure 8*a*).

The observed structures resemble dendrites. The orientation of each array as a whole along the *Y*-crystallographic directions is lost partially, while the local symmetry is still preserved (figure 8*b*). This effect can be attributed to the loss of long-range order, because this kinetic process develops under highly non-equilibrium conditions induced by the super-strong backswitching field.

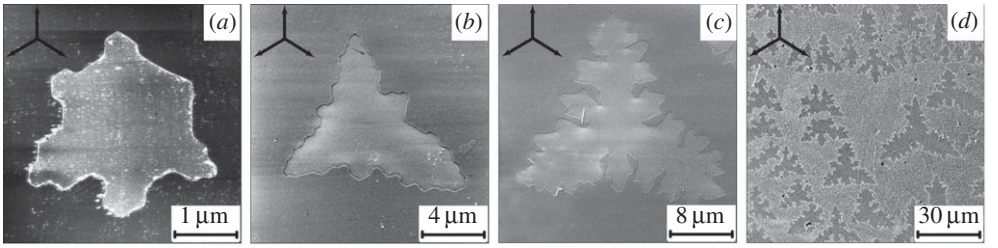

Figure 9. SEM images of the dendrite domain structures in MgO : LN revealed by etching after partial polarization reversal at an elevated temperature, $T = 250^{\circ}$C. (Reprinted with permission from Shur *et al.* [60]. Copyright © 2012, AIP Publishing LLC.)

The alternative scenario of backward wall motion is realized through the formation and propagation of the quasi-regular structure of fingers strictly oriented along the allowed Y directions, which differ for different sides of the stripe domain (figure 8*c*). The fingers grow towards each other, but the electrostatic interaction between the approaching and neighbouring fingers prevents their merging [3]. As a result, the 'dendrite-like' stable structure of residual domains remains after the termination of backswitching (figure 8*d*). The complicated shape of individual fingers is caused by a branching effect. It can be seen from the detailed analysis of the images that the branches are oriented along the permitted Y directions only. The higher mobility of the finger structure front when compared with that of the plane domain wall is due to the diminishing deceleration effect for the quasi-periodic distribution of bound charges [20,23].

The formation of the dendrite-like domain shapes has been investigated in the SLN crystals during polarization reversal at temperatures above 230°C (figure 9) [60]. After partial switching, the isolated domains of the complicated shape with typical sizes from 3 to 30 µm were distributed over the whole $Z+$ polar surface covered by an evaporated 80-nm-thick chromium electrode. The shape of the domain ensembles was close to that of a six-ray star with vertices oriented strictly along all six Y directions (figure 9*a–c*). It should be pointed out that $Y+$ oriented rays are essentially longer than $Y-$ oriented ones. This effect can be attributed to the difference in screening rates for $Y+$ and $Y-$ crystallographic directions in LN. The irregular domain shape demonstrates the loss of the domain shape stability (figure 9*b*,*c*). This effect leads to the formation of dendrite domain structures as a result of application of several field pulses (figure 9*c*,*d*).

The domain structure evolution of non-through domains that appeared at the polar surface was reconstructed by analysis of the set of CRM domain images obtained at different depths [45]. These data allowed us to reveal two mechanisms of dendrite domain structure formation during application of a single pulse with increasing field (figure 10). Discrete switching and domain merging were obtained at low field (figure 10*a–c*), while continuous domain growth was obtained at high field (figure 10*d–f*).

The following stages of dendrite structure formation for application of the single pulse were revealed (figure 10) [60]. (i) Appearance of the first isolated domain. (ii) Appearance of three isolated domains at equal distances from the first one in the $Y+$ directions, suppressing its further growth. (iii) Appearance of three isolated domains at equal distances from the central domain in the $Y-$ directions. (iv) Growth of the oriented domain chains with a sub-micrometre period in the $Y+$ directions. (v) Formation of six-ray stars as a result of domain merging. (vi) Broadening of star-like domain rays.

The application of several consecutive field pulses leads to the formation of dendrite domains with a more complex shape (figure 11), which can also be explained in the approach mentioned above.

The experimental results obtained allowed us to suggest a mechanism for self-organized formation of dendrite domain structures. It was shown that the framework of the dendrite structure appeared due to the formation of isolated domains and subsequent oriented growth of the nanodomain chains (discrete switching). The nanodomain period in the chains was defined

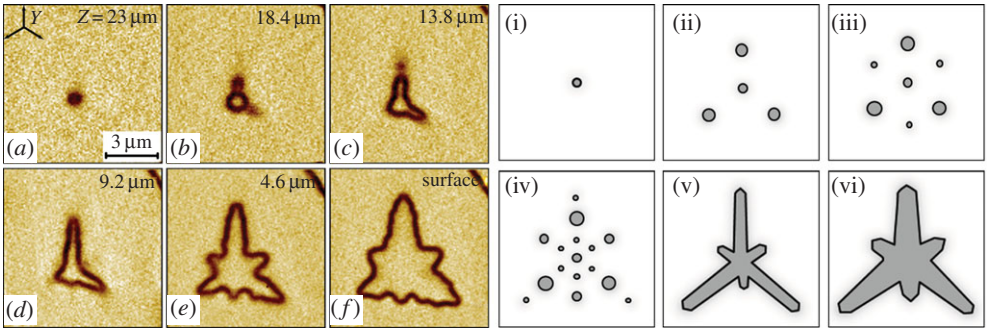

Figure 10. (*a–f*) Domain structure evolution during the application of a single pulse extracted from CRM images at different depths. (i)–(vi) Scheme of dendrite formation. (Reprinted with permission from Shur *et al.* [60]. Copyright © 2012, AIP Publishing LLC.) (Online version in colour.)

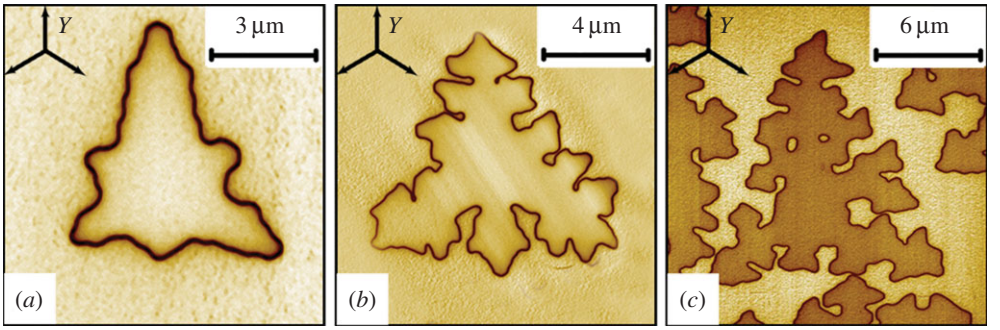

Figure 11. PFM images of dendrite domain structures for various numbers of field pulses: (*a*) single, (*b*) double and (*c*) triple. $E_{max} = 1.5$ kV mm^{-1}. (Reprinted with permission from Shur *et al.* [60]. Copyright © 2012, AIP Publishing LLC.) (Online version in colour.)

by the correlated nucleation effect [3,5]. It was shown by computer simulation that the period of the chain of isolated needle-like domains with charged domain walls was defined by the length of the last domain in the chain [62].

Switching at elevated temperatures was stimulated by stochastic nucleation instead of the determined nucleation at low temperatures. Independent domain growth after merging in this case resulted in dendrite domain shapes. Substitution of the dominating nucleation mechanism at the elevated temperature can be attributed to a change in the mechanism of electrical conductivity from anisotropic electronic to isotropic ionic.

The formation of the dendrite domain structures was observed in CLN with a polar surface modified by implantation of Ar ions as a result of polarization reversal under the application of a high external field (figure 12*a*) [46]. The modified surface layer leads to ineffective screening of the depolarization field, which is crucial for dendrite domain growth.

The formation of self-organized dendrite domain structures that appeared as a result of polarization reversal in low uniform external fields ranging from 20.2 to 21.2 kV mm^{-1} has been studied in CLN single crystals with a 1.5-µm-thick artificial surface dielectric layer created by the PE method [63]. The growth of hexagonal domains with walls oriented along the *Y*-crystallographic directions has been revealed by *in situ* optical visualization. The high-resolution PFM visualization of the static domain structures after partial polarization reversal revealed the self-organized sub-micrometre scale dendrite domain patterns consisting of domain stripes oriented along the *X*-crystallographic directions separated by arrays of dashed residual domains (figure 12*b–d*).

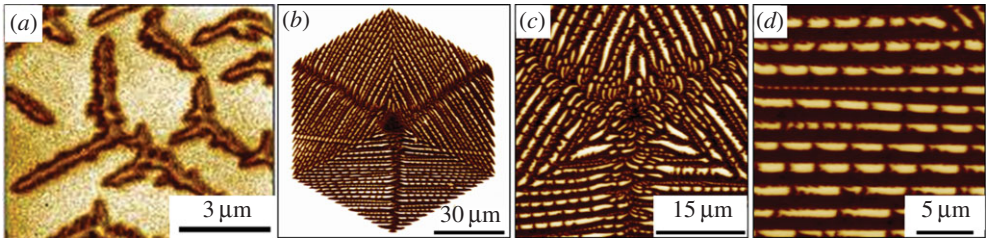

Figure 12. Dendrite domains in CLN with modified surface layers: (*a*) by implantation of Ar ions (CRM image); (*b–d*) by PE. PFM image, phase signal. Dark area corresponds to the switched domains. (Reprinted with permission from Shur *et al.* [63]. Copyright © 2017, AIP Publishing LLC.) (Online version in colour.)

The domain stripes are formed as a result of branching of three *Y*-oriented rays. The branching period is about 2 µm, which is close to the thickness of the PE layer. This process leads to the formation of the self-organized stripe structure. The period of the dashed structure ranged from 2 to 3 µm. The quasi-regular dendrite domain patterns with similar geometry were observed by CRM in the vicinity of both polar surfaces. The depth of the structure was about 20 µm for the *Z*+ polar surface and 70 µm for the Z− one.

10. Conclusion

The formation of the domain shape instabilities and self-similar domain structures, during polarization reversal in several uniaxial ferroelectrics in highly non-equilibrium switching conditions, has been studied in detail. The complementary methods of domain structure visualization have been used for the investigation of micro- and nanoscale static domain structures and domain kinetics in model uniaxial ferroelectrics: lithium niobate and lithium tantalate.

Modifications of the surface layer and spontaneous backswitching have been used for realization of the highly non-equilibrium switching conditions. Various manifestations of the discrete switching process through formation of the nanodomain arrays have been demonstrated. Original scenarios of the domain evolution including growth of the fractal, finger and dendrite domain structures were revealed experimentally and discussed within the unified kinetic approach, accounting for the decisive role of the retardation of the screening process. Various scenarios of dendrite domain growth were realized. Thus, evolution of the domain structure in uniaxial ferroelectrics can be considered as the model for the investigation of dendrite growth.

Data accessibility. This article has no additional data.

Authors' contributions. V.Ya.S. and A.R.A. wrote this in a joint effort.

Competing interests. We declare we have no competing interests.

Funding. The authors acknowledge support by the Russian Scientific Foundation (grant no. 14-12-00826).

Acknowledgements. It is a pleasure to acknowledge the helpful discussions with A.L. Korzhenevskii and E.L. Rumyantsev. The equipment of the Ural Center for Shared Use 'Modern nanotechnology' UrFU was used.

References

1. Feder J. 1988 *Fractals*. New York, NY: Plenum.
2. Shur VYa. 1996 Fast polarization reversal process: evolution of ferroelectric domain structure in thin films. In *Ferroelectric thin films: synthesis and basic properties. Ferroelectricity and related phenomena*, vol. 10 (eds CA Paz de Araujo, JF Scott, GW Taylor), pp. 153–192. Amsterdam, The Netherlands: Gordon & Breach Science Publ.
3. Shur VYa. 2005 Correlated nucleation and self-organized kinetics of ferroelectric domains. In *Nucleation theory applications* (ed. JWP Schmelzer), pp. 178–214. Weinheim, Germany: Wiley-VCH.

4. Shur VYa. 2006 Kinetics of ferroelectric domains: application of general approach to $LiNbO_3$ and $LiTaO_3$. *J. Mater. Sci.* **41**, 199–210. (doi:10.1007/978-0-387-38039-1_18)
5. Shur VYa. 2008 Nano- and micro-domain engineering in normal and relaxor ferroelectrics. In *Handbook of advanced dielectric, piezoelectric and ferroelectric materials. Synthesis, properties and applications*, (ed. Z-G Ye), pp. 622–669. Cambridge, UK: Woodhead Publishing Ltd.
6. Shur VYa, Rumyantsev EL, Nikolaeva EV, Shishkin EI, Fursov DV, Batchko RG, Eyres LA, Fejer MM, Byer RL. 2000 Nanoscale backswitched domain patterning in lithium niobate. *Appl. Phys. Lett.* **76**, 143–154. (doi:10.1063/1.125683)
7. Shur VYa *et al.* 2004 Self-organization in $LiNbO_3$ and $LiTaO_3$: formation of micro- and nano-scale domain patterns. *Ferroelectrics* **304**, 111–116. (doi:10.1080/00150190490457636)
8. Shur VYa *et al.* 2001 Formation of self-organized nanodomain patterns during spontaneous backswitching in lithium niobate. *Ferroelectrics* **253**, 105–114. (doi:10.1080/00150190108008448)
9. Shur VYa *et al.* 2007 Nanoscale domain effects in ferroelectrics. Formation and evolution of self-assembled structures in $LiNbO_3$ and $LiTaO_3$. *Ferroelectrics* **354**, 145–157. (doi:10.1080/00150190701454818)
10. Batchko RG, Shur VYa, Fejer MM, Byer RL. 1999 Backswitch poling in lithium niobate for high-fidelity domain patterning and efficient blue light generation. *Appl. Phys. Lett.* **75**, 1673–1675. (doi:10.1063/1.124787)
11. Merz W. 1954 Domain formation and domain wall motions in ferroelectric $BaTiO_3$ single crystals. *Phys. Rev.* **95**, 690–698. (doi:10.1103/PhysRev.95.690)
12. Balke N, Gajek M, Tagantsev AK, Martin LW, Chu Y-H, Ramesh R, Kalinin SV. 2010 Direct observation of capacitor switching using planar electrodes. *Adv. Funct. Mater.* **20**, 3466–3475. (doi:10.1002/adfm.201000475)
13. Kuroda A, Kurimura S, Uesu Y. 1996 Domain inversion in ferroelectric MgO:$LiNbO_3$ by applying electric fields. *Appl. Phys. Lett*. **69**, 1565–1567. (doi:10.1063/1.117031)
14. Chernykh A, Shur V, Nikolaeva E, Shishkin E, Shur A, Terabe K, Kurimura S, Kitamura K, Gallo K. 2005 Shapes of isolated domains and field induced evolution of regular and random 2D domain structures in $LiNbO_3$ and $LiTaO_3$. *Mater. Sci. Eng. B* **120**, 109–113. (doi:10.1016/j.mseb.2005.02.007)
15. Lobov AI, Shur VYa, Baturin IS, Shishkin EI, Kuznetsov DK, Shur AG, Dolbilov MA, Gallo K. 2006 Field induced evolution of regular and random 2D domain structures and shape of isolated domains in $LiNbO_3$ and $LiTaO_3$. *Ferroelectrics* **341**, 109–116. (doi:10.1080/00150190600896994)
16. Shur VYa, Nikolaeva EV, Shishkin EI, Chernykh AP, Terabe K, Kitamura K, Ito H, Nakamura K. 2002 Domain shape in congruent and stoichiometric lithium tantalate. *Ferroelectrics* **269**, 195–200. (doi:10.1080/00150190211168)
17. Shur VYa, Lobov AI, Shur AG, Rumyantsev EL, Gallo K. 2007 Evolution of isolated micro-domains in lithium niobate. *Ferroelectrics* **360**, 111–119. (doi:10.1080/00150190701517580)
18. Dolbilov MA, Shishkin EI, Shur VYa, Tascu S, Baldi P, De Micheli MP. 2010 Abnormal domain growth in lithium niobate with surface layer modified by proton exchange. *Ferroelectrics* **398**, 108–114. (doi:10.1080/00150193.2010.489840)
19. Kholkin AL, Bdikin IK, Shvartsman VV, Pertsev NA. 2007 Anomalous polarization inversion in ferroelectrics via scanning force microscopy. *Nanotechnology* **18**, 095502. (doi:10.1088/0957-4484/18/9/095502)
20. Fatuzzo E, Merz WJ. 1967 *Ferroelectricity*. Amsterdam, The Netherlands: North-Holland Publishing Company.
21. Miller RC, Weinreich G. 1960 Mechanism for the sidewise motion of 180° domain walls in barium titanate. *Phys. Rev.* **117**, 1460–1466. (doi:10.1103/PhysRev.117.1460)
22. Cahn JW. 1960 Theory of crystal growth and interface motion in crystalline materials. *Acta Metall.* **8**, 554–562. (doi:10.1016/0001-6160(60)90110-3)
23. Lines ME, Glass AM. 1977 *Principles and applications of ferroelectrics and related materials*. Oxford, UK: Clarendon Press.
24. Tagantsev AK, Cross LE, Fousek J. 2010 *Domains in ferroic crystals and thin films*. New York, NY: Springer.
25. Sluka T, Tagantsev AK, Bednyakov P, Setter N. 2013 Free-electron gas at charged domain walls in insulating $BaTiO_3$. *Nat. Commun.* **4**, 1808. (doi:10.1038/ncomms2839)

26. Shur VYa, Rumyantsev EL, Nikolaeva EV, Shishkin EI. 2000 Formation and evolution of charged domain walls in congruent lithium niobate. *Appl. Phys. Lett.* **77**, 3636–3638. (doi:10.1063/1.1329327)
27. Fridkin VM. 1980 *Ferroelectric semiconductors*. New York, NY: Consultants Bureau.
28. Shur VYa, Gruverman AL, Rumyantsev EL. 1990 Dynamics of domain structure in uniaxial ferroelectrics. *Ferroelectrics* **111**, 123–131. (doi:10.1080/00150199008224389)
29. Lambeck PV, Jonker GH. 1986 The nature of domain stabilization in ferroelectric perovskites. *J. Phys. Chem. Solids* **47**, 453–461. (doi:10.1016/0022-3697(86)90042-9)
30. Tagantsev AK, Stolichnov I, Colla EL, Setter N. 2001 Polarization fatigue in ferroelectric films: basic experimental findings, phenomenological scenarios, and microscopic features. *J. Appl. Phys.* **90**, 1387–1402. (doi:10.1063/1.1381542)
31. Prokhorov AM, Kuz'minov YS. 1990 *Physics and chemistry of crystalline lithium niobate*. New York, NY: Hilger.
32. Kitamura K, Furukawa Y, Niwa K, Gopalan V, Mitchell TE. 1998 Crystal growth and low coercive field 180° domain switching characteristics of stoichiometric $LiTaO_3$. *Appl. Phys. Lett.* **73**, 3073–3075. (doi:10.1063/1.122676)
33. Niwa K, Furukawa Y, Takekawa S, Kitamura K. 2000 Growth and characterization of MgO doped near stoichiometric $LiNbO_3$ crystals as a new nonlinear optical material. *J. Crystal Growth* **208**, 493–500. (doi:10.1016/S0022-0248(99)00450-9)
34. Soergel E. 2005 Visualization of ferroelectric domains in bulk single crystals. *Appl. Phys. B* **81**, 729–751. (doi:10.1007/s00340-005-1989-9)
35. Shur VYa, Zelenovskiy PS. 2014 Micro- and nanodomain imaging in uniaxial ferroelectrics: joint application of optical, confocal Raman and piezoelectric force microscopy. *J. Appl. Phys.* **116**, 066802. (doi:10.1063/1.4891397)
36. Shur VYa, Lobov AI, Shur AG, Kurimura S, Nomura Y, Terabe K, Liu XY, Kitamura K. 2005 Rearrangement of ferroelectric domain structure induced by chemical etching. *Appl. Phys. Lett.* **87**, 022905. (doi:10.1063/1.1993769)
37. Alexe M, Gruverman A. 2004 *Nanoscale characterisation of ferroelectric materials. Scanning probe microscopy approach*. New York, NY: Springer.
38. Kalinin SV, Gruverman A (eds). 2007 *Scanning probe microscopy. Electrical and electromechanical phenomena at the nanoscale*. New York, NY: Springer Science + Business Media, LLC.
39. Gruverman A, Kalinin SV. 2006 Piezoresponse force microscopy and recent advances in nanoscale studies of ferroelectrics. *J. Mater. Sci.* **41**, 107–116. (doi:10.1007/s10853-005-5946-0)
40. Kalinin SV, Morozovska AN, Chen LQ, Rodriguez BJ. 2010 Local polarization dynamics in ferroelectric materials. *Reports Prog. Phys.* **73**, 056502. (doi:10.1088/0034-4885/73/5/056502)
41. Kalinin S, Rar A, Jesse S. 2006 A decade of piezoresponse force microscopy: progress, challenges, and opportunities. *IEEE Trans. Ultrason. Ferroelectr. Freq. Control* **53**, 2226–2252. (doi:10.1109/TUFFC.2006.169)
42. Kalinin S, Bonnell D. 2002 Imaging mechanism of piezoresponse force microscopy of ferroelectric surfaces. *Phys. Rev. B* **65**, 125408. (doi:10.1103/PhysRevB.65.125408)
43. Balke N, Bdikin I, Kalinin SV, Kholkin AL. 2009 Electromechanical imaging and spectroscopy of ferroelectric and piezoelectric materials: state of the art and prospects for the future. *J. Am. Ceram. Soc.* **92**, 1629–1647. (doi:10.1111/j.1551-2916.2009.03240.x)
44. Bonnell DA, Kalinin SV, Kholkin AL, Gruverman A. 2009 Piezoresponse force microscopy: a window into electromechanical behavior at the nanoscale. *MRS Bull.* **34**, 648–657. (doi:10.1557/mrs2009.176)
45. Shur V, Shikhova V, Ievlev A, Zelenovskiy P, Neradovskiy M, Pelegov D, Ivleva L. 2012 Nanodomain structures formation during polarization reversal in uniform electric field in strontium barium niobate single crystals. *J. Appl. Phys.* **112**, 064117. (doi:10.1063/1.4754511)
46. Shur VYa, Shishkin EI, Nikolaeva EV, Nebogatikov MS, Alikin DO, Zelenovskiy PS, Sarmanova MF, Dolbilov MA. 2010 Study of nanoscale domain structure formation using Raman confocal microscopy. *Ferroelectrics* **398**, 91–97. (doi:10.1080/00150193.2010.489838)
47. Zelenovskiy PS, Shur VYa, Bourson P, Fontana MD, Kuznetsov DK, Mingaliev EA. 2010 Raman study of neutral and charged domain walls in lithium niobate. *Ferroelectrics* **398**, 34–41. (doi:10.1080/00150193.2010.489810)

48. Shur VYa, Zelenovskiy PS, Nebogatikov MS, Alikin DO, Sarmanova MF, Ievlev AV, Mingaliev EA, Kuznetsov DK. 2011 Investigation of the nanodomain structure formation by piezoelectric force microscopy and Raman confocal microscopy in $LiNbO_3$ and $LiTaO_3$ crystals. *J. Appl. Phys.* **110**, 052013. (doi:10.1063/1.3623778)
49. Hammoum R, Fontana MD, Bourson P, Shur VYa. 2007 Raman micro-spectroscopy as a probe to investigate PPLN structures. *Ferroelectrics* **352**, 106–110. (doi:10.1080/00150190701358191)
50. Hammoum R, Fontana MD, Bourson P, Shur VYa. 2008 Characterization of PPLN-microstructures by means of Raman spectroscopy. *Appl. Phys. A* **91**, 65–67. (doi:10.1007/s00339-007-4356-3)
51. Capek P, Stone G, Dierolf V, Althouse C, Gopalan V. 2007 Raman studies of ferroelectric domain walls in lithium tantalate and niobate. *Phys. Status Solidi C* **4**, 830–833. (doi:10.1002/pssc.200673720)
52. Zelenovskiy PS, Shikhova VA, Ievlev AV, Neradovskiy MM, Shur VYa. 2012 Micro-Raman visualization of domain structure in strontium barium niobate single crystals. *Ferroelectrics* **439**, 33–39. (doi:10.1080/00150193.2012.746890)
53. Zelenovskiy PS, Fontana MD, Shur VYa, Bourson P, Kuznetsov DK. 2010 Raman visualization of micro- and nanoscale domain structures in lithium niobate. *Appl. Phys. A* **99**, 741–744. (doi:10.1007/s00339-010-5621-4)
54. Hayashi M. 1972 Kinetics of domain wall motion in ferroelectric switching. Pt. 1. General formulation. *J. Phys. Soc. Jpn.* **33**, 616–628. (doi:10.1143/JPSJ.33.616)
55. Shur VYa, Shur AG, Akhmatkhanov AR. 2017 Formation of self-assembled micro- and nano-domain structures in uniaxial ferroelectrics. *IOP Conf. Ser. Mater. Sci. Eng.* **192**, 12006. (doi:10.1088/1757-899X/192/1/012006)
56. Dolbilov MA, Shur VYa, Shishkina EV, Angudovich ES, Ushakov AD, Baldi P, De Micheli MP. 2013 Formation of nanodomain structure in front of the moving domain wall in lithium niobate single crystal modified by proton exchange. *Ferroelectrics* **442**, 82–91. (doi:10.1080/10584587.2013.776408)
57. Shur VYa, Gruverman AL, Ponomarev NYU, Tonkachyova NA. 1992 Change of domain structure of lead germanate in strong electric field. *Ferroelectrics* **126**, 371–376. (doi:10.1080/00150199208227088)
58. Shur VYa, Gruverman AL, Ponomarev NYU, Rumyantsev EL, Tonkachyova NA. 1991 Domain structure kinetics in ultrafast polarization switching in lead germanate. *JETP Lett.* **53**, 615–619.
59. Shur VYa, Akhmatkhanov AR, Chezganov DS, Baturin IS, Smirnov MM. 2013 Shape of isolated domains in lithium tantalate single crystals at elevated temperatures. *Appl. Phys. Lett.* **103**, 242903. (doi:10.1063/1.4846015)
60. Shur VYa, Chezganov DS, Nebogatikov MS, Baturin IS, Neradovskiy MM. 2012 Formation of dendrite domain structures in stoichiometric lithium niobate at elevated temperatures. *J. Appl. Phys.* **112**, 104113. (doi:10.1063/1.4766308)
61. Weis RS, Gaylord TK. 1985 Lithium niobate: summary of physical properties and crystal structure. *Appl. Phys. A* **37**, 191–203. (doi:10.1007/BF00614817)
62. Shur VYa, Lobov AI, Rumyantsev EL, Kuznetsov DK. 2010 3D modeling of domain structure evolution during discrete switching in lithium niobate. *Ferroelectrics* **399**, 68–75. (doi:10.1080/00150193.2010.490291)
63. Shur VYa, Akhmatkhanov AR, Chuvakova MA, Dolbilov MA, Zelenovskiy PS, Lobov AI. 2017 Formation of self-organized domain structures with charged domain walls in lithium niobate with surface layer modified by proton exchange. *J. Appl. Phys.* **121**, 104101. (doi:10.1063/1.4978014)